DR SUBODH GANESANPOTTI (Orcid ID : 0000-0002-6784-094X)

Article type : Article

Crystal Structure, Phonon Modes, and Bond Characteristics of $AgPb_2B_2V_3O_{12}$ (B=Mg, Zn) Microwave Ceramics

Rakhi M. and Subodh G.*

Department of Physics

University of Kerala

Thiruvananthapuram-695581

Kerala, India.

*gsubodh@gmail.com

ABSTRACT

$AgPb_2B_2V_3O_{12}$ (B=Mg, Zn) ceramics with low sintering temperature were synthesized via the conventional solid-state reaction route. Rietveld refinements of the X-ray diffraction patterns confirm cubic symmetry with space group $Ia\,\bar{3}$d. The number of observed vibrational modes and those predicted by group theoretical calculations also confirm the $Ia\,\bar{3}$d space group. At the optimum sintering temperature of 750°C/4h, $AgPb_2Mg_2V_3O_{12}$ has a relative permittivity of 23.3 ± 0.2, unloaded quality factor ($Q_u \times f$) of $26{,}900 \pm 500$ GHz ($f = 7.57$ GHz) and temperature coefficient of resonant frequency of 19.3 ± 1 ppm/°C, while $AgPb_2Zn_2V_3O_{12}$ has the corresponding values of

This article has been accepted for publication and undergone full peer review but has not been through the copyediting, typesetting, pagination and proofreading process, which may lead to differences between this version and the Version of Record. Please cite this article as doi: 10.1111/JACE.16991

26.4 ± 0.2, $28{,}400 \pm 500$ GHz($f = 7.21$ GHz) and -18.4 ± 1 ppm/^{o}C at 590^{o}C/4h. Microwave dielectric properties of a few reported garnets and $Pb_2AgB_2V_3O_{12}$ (B=Mg, Zn) ceramics were correlated with their intrinsic characteristics such as the Raman shifts as well as width of A_{1g} Raman bands. Higher quality factor were obtained for lower full width at half-maxima (FWHMs) values of A_{1g} modes. The increase in B-site bond valence contributes to high $Q_u \times f$ and low $|\tau_f|$ with the substitution of Zn^{2+} by Mg^{2+}. Further, the high ionic polarizability and unit cell volume with Zn^{2+}substitution contribute to increased relative permittivity.

Keywords: crystal structure, Raman spectra, garnet, microwave dielectric properties, bond valence

1. INTRODUCTION

Modern communication systems demand newly developed microwave dielectric materials for fabricating filters, resonators, dielectric substrates, oscillators, antennas, guided wave circuits, etc. because of their compactness, light weight, thermal stability, low cost of production, better efficiency, and adaptability to microwave integrated circuits. These types materials have immense applications in the fields of mobile phones, radars, satellite broadcasting, global positioning system, etc. A microwave dielectric ceramic should possess some stringent properties such as (i) high unloaded quality factor ($Q_u \times f$) for better selectivity, (ii) high relative permittivity (ε_r) for miniaturization,(iii) zero temperature coefficient of the resonant frequency (τ_f) for temperature stability and (iv) low sintering temperature. The development of materials that combine all the above-mentioned properties has become a key challenge for the electronic industry.[1-8]

Literature provides many dielectric materials with excellent microwave properties, which include Li_2O, TeO_2, MoO_3, P_2O_5, and Bi_2O_3[9-16]-rich compounds and silicate ceramic materials such as Zn_2SiO_4, Al_2SiO_5, Mg_2SiO_4, $Sr_2Al_2SiO_7$, etc. [17-20] Even though Si- and Al-containing compounds show better dielectric properties ,their high sintering temperature (>1300^{o}C) preclude their applications in microwave circuits. Recently, materials containing V^{5+} ions are studied owing to their applications in a wide range of areas such as catalysis, phosphors, biochemistry, electrochemistry etc.[21-25] Vanadium-containing compounds are also considered useful for future microwave applications because of their high Q factor, appropriate relative permittivity, low cost, and low

sintering temperatures. Wang et al.[26] reported the microwave dielectric properties of BVO_4 (B=La, Ce) ceramics as ε_r=14.2 and 12.3, $Q_u \times f = 48{,}197$ and 41,460 GHz and $\tau_f = -37.9$ and -34.4 ppm/°C, respectively, for $LaVO_4$ and $CeVO_4$. Li et al.[27] reported that $Ca_5Co_4V_{5.95}O_{24}$–$0.1TiO_2$ ceramic has a relative permittivity of 13.7, $Q_u \times f = 19{,}159$ GHz and $\tau_f = 0$ ppm/℃. At the optimum sintering temperature of 875 °C, $Ca_5Mn_4(VO_4)_6$ ceramic showed a relative permittivity of 11.2, $Q_u \times f = 33{,}800$ GHz, and $\tau_f = -70$ ppm/℃.[28] Further, a few AgO-rich compounds have been recently reported with excellent microwave properties with low sintering temperature. Zhou et al.[29] reported that $(Na_{1.2}Ag_{0.8})MoO_4$ ceramic sintered at 410 °C possesses a relative permittivity of 8.1, quality factor of 44,800 GHz and temperature coefficient of the resonant frequency of -82 ppm/°C.

Moreover, recently various vanadate-based garnet materials have been studied as new rare earth-free dielectric materials. These garnets have the general composition $A_3B_2C_3O_{12}$, which provides three different sites (A, B and C) for a wide variety of cation substitutions. Whereas the C ions are surrounded by four oxygen ions to form CO_4 tetrahedra, the B-site ions form octahedral coordination with the oxygen atoms. The corner-shared tetrahedra and octahedra form dodecahedra, where the A-site ions are located[30]. These structures can include a wide variety of chemical substitutions, which include $A_2^{I}REM_2V_3O_{12}$, $A^{II}5M_4V_6O_{24}$ and $A^{I}A_2^{II}M_2V_3O_{12}$ (A^{I}=alkali metals and Ag, A^{II}= alkali earth metals; RE= Sc, Y and lanthanides, M=Mg, Zn)[31]. Fang et al. reported that $NaCa_2Mg_2V_3O_{12}$ sintered at 915 °C/4h has a relative permittivity =10, $Q_u \times f = 50{,}600$ GHz and $\tau_f = -47$ ppm/℃.[32]Another compound $LiCa_3MgV_3O_{12}$, has a relative permittivity =10, $Q_u \times f = 74{,}700$ GHz and $\tau_f = -61$ ppm/℃.[33] Yao et al. studied $Ca_5Mg_4(VO_4)_6$ sintered at 800 °C, which was found to have relative permittivity = 9.2, $Q_u \times f = 53{,}300$ GHz and $\tau_f = -80$ ppm/℃.[34] Also recently Cheng et al.[35] reported two garnet compounds $AgCa_2B_2V_3O_{12}$(B=Mg, Zn) with $\varepsilon_r = 10.3$ and 11.2,$Q_u \times f = 43{,}000$ and 26,930 GHz and and $\tau_f = -69$ and –95 ppm/℃ respectively. More recently, we reported two ceramic compounds, $NaPb_2B_2V_3O_{12}$ (B=Mg,Zn) with $\varepsilon_r = 20.6$ and 22.4, unloaded quality factor ($Q_u \times f$) = 22,800 (f=7.7 GHz) and 7900 (f=7.4 GHz) and temperature coefficient of the resonant frequency = $+25.1$ and -6 ppm/℃, respectively[36]. In 2006, Iishi et al.[37] reported a series of novel garnets including $Pb_2AgB_2V_3O_{12}$ (B=Mg, Zn),but their microwave dielectric properties have not been investigated so far. While considering the better dielectric properties of $NaPb_2B_2V_3O_{12}$ (B=Mg, Zn) ceramics at low sintering temperatures and also the similar ionic radii of

Na^+ (1.18 Å) and Ag^+ (1.28 Å) for same co-ordination number (CN) =8, it was reasonable to study the microwave dielectric properties of $Pb_2AgB_2V_3O_{12}$(B=Mg, Zn) (hereafter called APMVO and APZVO) ceramics. It was also worth to investigate the correlation between microwave dielectric properties and structural characteristics such as Raman shifts and width of Raman bands for all the reported garnet compounds. Further, for APMVO and APZVO, correlations between microwave dielectric properties, bond valence and packing fraction were also studied.

2. EXPERIMENTAL

Material Synthesis and Characterization

High-density samples were synthesized through a conventional solid-state reaction route using high-purity powders of Ag_2CO_3 (Sigma Aldrich, 99.5%), ZnO, MgO, PbO and NH_4VO_3 (Sigma Aldrich >99%). First, MgO was heated at 900°C/2h to remove the moisture in the sample. Then the reagents were ball-milled using ceria-stabilized zirconia balls in acetone medium for 24 h. After drying, the uniform mixture was placed in an alumina crucible and calcined at 625 and 550°C for 4h respectively, for APMVO and APZVO. For dielectric measurements, the calcined powders were ground and mixed with 5wt% PVA solution. Then the slurries were dried and pressed into cylindrical pellets with a diameter of 10 mm and thickness of about 2 and 5 mm for radio and microwave frequency dielectric measurements respectively. The density of the pellets was measured using the Archimedes method. The green pellets were sintered at the optimum sintering temperatures of 750 °C/4h and 590 °C/4h for APMVO and APZVO respectively. The microstructures were studied using a pellet of 1 mm thickness polished and etched 25 °C below their optimum sintering temperature.

The phase purity and crystal structure of the synthesized compounds were investigated by X-ray Diffractometer (XRD) using Cu Kα radiation (λ = 1.5406 Å) in a Bruker D8 Advance Diffractometer. Rietveld refinements of the XRD patterns of the compounds were carried out using the Topas 4.2 software. The room temperature Raman spectra were recorded using a LABRAM HR 800 Raman spectrometer with excitation wavelength of 514.5 nm in the spectral range from 100 to 1000 cm^{-1} and having spectral resolution of 1 cm^{-1}. Before fitted with the lorentzian function the raw Raman data were first corrected using the Bose–Einstein thermal population factor given as:

$$I_{red} = I_{obt}[1 - \exp(\frac{-hc\vartheta)}{KT})]\frac{\vartheta{\vartheta_0}^3}{(\vartheta_0 - \vartheta)^4} \qquad (1)$$

Where I_{red},I_{obt} indicate the reduced and obtained Raman intensity. The term h, c,ϑ, ϑ_0, K, T represent the Planck's constant, velocity of light, Raman shift, wave number corresponds to the excitation wave length, Boltzmann constant and temperature in Kelvin scale [38]. The Lorentzian function used to fit the Raman data was given as follows :

$$y = yo + \frac{2A}{\pi} \times \left(\frac{W}{4(\vartheta - \vartheta_C)^2 + W^2}\right) \quad (2)$$

Where yo, A, ϑ_C and w corresponds to the offset, area, center and FWHM values. The infrared reflectivity spectra of the compounds were measured using a JASCOFTIR 6800 spectrometer at room temperature. Fourier transform infrared (FTIR) data were obtained in the attenuated total reflection (ATR) mode with a resolution of 1 cm^{-1}.The surface morphology of the compounds was analyzed using a scanning electron microscope (ZEISS EVO 18). Radio frequency dielectric measurements were carried out using an LCR meter (HIOKI 6582) and the microwave dielectric properties were measured using a vector network analyzer (ROHDE & SCHWARZ, ZV-Z135). The $TE_{01\delta}$ mode cavity method was adopted to find out the relative permittivity and unloaded quality factor of the compounds. The temperature coefficient of the resonant frequency (τ_f) was calculated by noting the variations of the $TE_{01\delta}$ mode frequency in the temperature range 25–85°C, using the following formula:

$$\tau_f = \frac{f_{85} - f_{25}}{60 \times f_{25}} \times 10^6 \quad (3)$$

where $f_{85}$and f_{25} are the resonant frequencies at 85 and 25 °C, respectively.

3. RESULTS AND DISCUSSION

3.1 Crystal structure

Figure S1 shows the XRD patterns of APMVO and APZVO ceramics calcined at 625 and 550 °C, respectively. Both compounds show a cubic garnet structure with the space group $Ia\,\bar{3}d$. All reflections are well matched with the ICDD file No.00-024-1104. The absence of any additional reflections confirmed the single-phase nature of the compounds. In order to study the crystal structure in detail, Rietveld refinements of the XRD patterns of the compounds were carried out, which are shown in Figures 1 and 2. The refinement of the XRD patterns of the samples showed good reliability

factors and χ^2 values. The obtained refinement parameters are Rp=3.88%, Rwp=5.63% and goodness of fit =1.94 for APMVO, Rp=4.45%, Rwp=5.97% and goodness of fit =1.24 for APZVO. The refined crystallographic parameters are listed in Table S1.The unit cell volumes were 2081and 2090Å^3 for B=Mg, Zn which indicates the increase in the lattice parameter and unit cell volume with the substitution of Zn^{2+} for Mg^{2+} ($r^{Mg^{2+}}$=0.72Å, $r^{Zn^{2+}}$=0.74Å). In the garnet structure of APMVO and APZVO, owing to the similar ionic radius of Pb (1.29Å) and Ag (1.28 Å), both atoms occupy the same 24*c* Wyckoff position, where they are coordinated dodecahedraly with oxygen atoms. The Mg/Zn atoms are located in the 16*a* sites with octahedral point symmetry (S_6) and the V atom occupies the 24*d* site with tetrahedral point symmetry (S_4). The oxygen atoms occupy in the 96h site, only by knowing the positions of oxygen atoms the crystal structure can be determined. All the other cations are occupied in their fixed positions. The position of oxygen in a garnet structure can be deduced using the following equations[31,36,39]:

$$\begin{cases} x = 0.0278\,r(A) + 0.0123\,r(B) - 0.0482\,r(C) + 0.0141 \\ y = -0.0237r(A) + 0.0200r(B) + 0.0321r(C) + 0.0523 \\ z = -0.0102r(A) + 0.0305r(B) - 0.0217r(C) + 0.6519 \end{cases} \quad (4)$$

Here *x*, *y*, and *z* represent the 96*h* site atomic position of an O atom. *A*, *B* and *C*are the ionic radii of the ions (expressed in Å). The calculated atomic position (*x*, *y*, *z*) for O in APMVO are (0.0415,0.0476 and 0.6530), whereas for APZVO the parameters are (0.0418,0.0480 and 0.6536). Table 1 and 2 show the obtained atomic coordinates for oxygen from Rietveld refinements, which almost match the theoretical values.

In this structure, each oxygen atom is shared by one VO_4 tetrahedra, one MgO_6/ZnO_6 octahedron and two equivalent dodecahedra. The insets of Figures 1 and 2 show the polyhedral representation of the crystal structure of APMVO and APZVO, where Ag^+ and Pb^{2+} randomly occupy the eight-coordinated A site, which is a three-dimensional network formed via the corner-sharing of tetrahedra and octahedra. The six-coordinated B sites are occupied by Mg^{2+} and Zn^{2+} ions, and V^{5+} is occupy the four-coordinated C sites. Table S2 shows the distance between the cations and the oxygen anions. The bonds V–O in *t*he $[VO_4]$ tetrahedra and B–O in *t*he $[BO_6]$ octahedra increase slightly with the substitution of Zn^{2+} for Mg^{2+} ions. A similar behavior, i.e., increase in bond length of the tetrahedra and octahedra with the substitution of Zn^{2+} for Mg^{2+}, was also reported in systems including

$Ca_5M_4(VO_4)_6$ (M = Zn and Mg)[40] and $LiCa_3MV_3O_{12}$ (M = Zn and Mg),[31] which is due to the larger ionic radius of Zn^{2+} ion.

3.2 Density and Micro structural Analysis

Figure 3 shows the dependence of the relative density and bulk density of APMVO and APZVO ceramics as a function of the sintering temperature. The theoretical (calculated) density of APMVO and APZVO is 5.81 and 6.33 g/cm^3, respectively. As the sintering temperature is increased from 675 to 750 ^{o}C, the bulk density also increases from 5.30 to 5.59 g/cm^3, and thereafter decreases to 5.48 g/cm^3 at 775 ^{o}C. APZVO also shows a similar trend of variation from 5.62 to 5.99 g/cm^3 when the temperature is increased from 560 to 590 ^{o}C, and then decreases to 5.78 g/cm^3 at 600 ^{o}C. At the optimum sintering temperature of 750^{o}C, APMVO shows the maximum bulk density of 5.59 g/cm^3 with the percentage density of 96.3 $\pm$ 0.1, while APZVO possess bulk density of 5.99 g/cm^3 with 94.6 $\pm$ 0.1 of percentage density at its optimum temperature of 590^{o}C. Usually, ceramics containing Zn^{2+} ions are sintered at lower temperatures compared to those containing Mg^{2+} ions.[31,35,36]

The microstructures of APMVO and APZVO sintered at the optimum sintering temperatures of 750 and 590 ^{o}C, respectively are shown in Figure 4. Both compounds show a dense and homogeneous microstructure with less porosity, which confirms its high density at the optimum sintering temperature. The average grain size is about 3.1 ($\pm$ 0.2) and about 3.9 ($\pm$ 0.4) μm for APMVO and APZVO, respectively. Moreover, the low melting nature of the compounds is evident from the larger grains possessed by the compounds. Especially in the case of APZVO, at its optimum sintering temperature it shows a decreased quality factor, which indicates the low melting nature of the compound.

3.3 Vibrational Spectra

Figures S2 and S3 show the Raman and FTIR spectra of the calcined compounds at room temperature. According to factor group analysis, a garnet structure has 98 vibrational modes at the Brillouin zone center, of which 55 are silent modes and one is an acoustic mode. The remaining are 25 Raman-active and 17 IR-active vibrations.[41-43]

$$\Gamma_{total} = 3A_{1g}+5A_{2g}+8E_g+14T_{1g}+14T_{2g}+5A_{1u}+5A_{2u}+10E_u+18T_{1u}+16T_{2u} \quad (5)$$

$\Gamma_{acoustic} = T_{1u}$

The 25 Raman active bands are $3A_{1g}+8E_g+14T_{2g}$, where A_{1g},E_g and T_{2g} represents the internal modes, translational modes and rotatory modes respectively. The IR-active bands are represented by one type of symmetry, namely T_{1u}. Figure 5 shows the deconvoluted Raman spectra of APMVO and APZVO ceramics. In a typical garnet structure, the Raman-active vibrational modes are divided into external and internal modes. The external modes are due to the translational motion of the cations, and the internal vibrations are associated with the vibrations of the $[VO_4]^{3-}$ tetrahedra. The modes with maximum intensity correspond to the stretching and bending vibrations of the VO_4 group, which are denoted as A_{1g}.[36] The modes below 250 cm^{-1} are mainly related to the external translational motion of Ag^{+}/ Pb^{+} and $(Mg^{2+}/Zn^{2+}) - O$ bonds. The internal bending vibrations of $[VO_4]^{3-}$ lie between 300 and 600 cm^{-1}, whereas the modes above 600 cm^{-1} correspond to the symmetric and asymmetric stretching of the $[VO_4]^{3-}$ group, which linearly depends on the lattice parameter .[36,44]

By using a Lorentzian function, 12 and 15 Raman-active bands can be fitted for APMVO and APZVO respectively, out of the 25 modes predicted by factor group analysis. Generally, the 17 IR-active vibrational modes consist of 3 asymmetric bends (ν_4), 3 asymmetric stretching modes corresponding to the tetrahedra (ν_3), 1 symmetric bend (ν_2), 2 translations and 2 rotations of the tetrahedra (R), 3 translations arising from the dodecahedra site (T_d), and 3 translations from the octahedral cations (T_o).[45] There are 12 and 14 IR-active bands observed for APMVO and APZVO respectively. Table S4 provides the detailed IR band assignments of APMVO and APZVO ceramics. Even though the Raman and IR spectra show fewer bands compared to theoretical predictions, the presence of characteristic bands of the garnet structure further confirms the symmetry of the compounds. The change in net polarizability, overlapping of bands, low resolving power of the instrument, polycrystalline nature of samples, etc. may be responsible for the reduced number of Raman-and IR-active bands found in these compounds.

3.4 Microwave Dielectric Properties

The variations in microwave dielectric properties (ε_r and $Q_u \times f$) of APMVO and APZVO ceramics with sintering temperature are shown in Figures 6 and 7, respectively. The relative permittivity of

both compounds increases up to their optimum sintering temperature, whereas beyond that temperature it decreases, similar to the variation of density. At the optimum sintering temperature, APMVO has a relative permittivity of 22.2 ± 0.2, and APZVO about 24.4 ± 0.2. The porosity-corrected relative permittivity is calculated using the Bosman and Havingas as follows [46]:

$$\varepsilon_{\text{Bosman}} = \varepsilon_{\text{m}}(1 + 1.5P) \qquad (6)$$

$$P = \left(1 - \frac{\rho_{\text{mea}}}{\rho_{\text{theo}}}\right)$$

where ε and $\varepsilon_{\text{m}}$are the porosity-corrected and measured relative permittivity respectively, and P is the fractional porosity. The porosity-corrected permittivities are listed in Table 3.

The dependence of $Q_u \times f$ with sintering temperature is same as that of relative permittivity and density. However, in the case of APZVO, at its optimum sintering temperature, it shows a slightly decreased $Q_u \times f$. Both intrinsic and extrinsic factors contribute to microwave dielectric loss. The microwave dielectric losses due to substitution, impurity, secondary phases, cavity, oxygen vacancies, poor density and grain sizes, etc. come under the category of extrinsic losses, while the losses arising from the variations occurring in lattice vibration modes and crystal structure are called intrinsic dielectric losses.[47] In our case, even though APZVO shows a higher density at its optimum sintering temperature, its $Q_u \times f$ is slightly lower, which could be attributed to its low melting nature.

3.5 Structural Characteristics and Microwave Dielectric Properties in Garnet Systems

The physical properties of materials depend on their crystal structure and bonding. In order to identify new compounds in the garnet system with excellent microwave dielectric properties, a closer analysis of the correlation between the structure and microwave dielectric properties of existing compounds is required. Hence, using available data from the literature about garnet-based systems, correlations between the crystal structures, bonding, and dielectric properties are established.

The relative permittivity of a compound is mainly influenced by its density, molar volume, and micro structural polarizability of the constituent ions.[48-49] In the present study, all the compounds have >94% of the theoretical density. So, the factors that affect the relative permittivity are intrinsic ones. Here, the Shannon additive rules were used to calculate the theoretical ionic polarizability as well as

the relative permittivity in order to understand the influence of crystal structure on the relative permittivity. In the case of $Pb_2AgB_2V_3O_{12}$ ceramics, the values were obtained as follows:

$$\alpha_{\text{theo}} = \alpha(Pb_2AgB_2V_3O_{12})$$

$$= \alpha\,(Ag^{2+}) + 2\alpha\,(Pb^{2+}) + 2\alpha\,(B^{2+}) + 3\alpha\,(V^{5+}) + 12\alpha\,(O^{2-})$$

where α (Ag^{2+}), α (Pb^{2+}), α (Mg^{2+}), α (Zn^{2+}), α (V^{5+}) and α (O^{2-}) are 2.25, 6.58, 1.33, 2.09, 2.92 and 2.01, respectively.[29,50] It was found that, in the case of APMVO, α_{theo} is about 50.93, while that of APZVO is about 52.47. The corresponding theoretical permittivity of single-phase compounds can be calculated using the Clausius-Mossotti equation as follows:

$$\varepsilon_r = \frac{8\pi\alpha_D + 3V_m}{3V_m - 4\pi\alpha_D} \qquad (7)$$

$$\alpha_{\text{obser}} = \frac{1}{b} V_m \frac{\varepsilon - 1}{\varepsilon + 2} \qquad (8)$$

where α_D is the theoretical polarizability and V_m is the molar volume of the compound. The theoretical polarizabilities of some reported garnets were also calculated using the Shannon additive rule. Figure S6 shows the variation of relative permittivity as a function of theoretical polarizability of some garnet compounds. It is generally accepted that, as theoretical polarizability increases, the relative permittivity also increases, which is also evident from the graph. The permittivity calculated using α_D is about 14.63 and 16.83 for APMVO and APZVO, respectively. The observed polarizability corresponding to the measured relative permittivity is about 54.42 and 55.33 for APMVO and APZVO, respectively. Table 3 shows the observed and theoretical values of α for the compounds. The "rattling" or "compressed" cation with high or low polarizability, the influence of dipolar impurities present in the compounds, etc. are the factors that cause the variation in the measured and calculated polarizability.[51]

The Raman shift and FWHM are the two important parameters through which the crystal structure and microwave dielectric properties can be correlated. Raman shift is related to the unit cell volume, while FWHM is related to the degree of cation ordering.[52] The equation connecting the Raman shift and $V-O$ bond length has the form $\vartheta = 21349\,\exp^{(-1.9176R)}$, in which ϑ is the Raman

shift and R is the bond length (i.e., $V-O$).[53] The decrease in Raman shift is attributed to the increase in the bond length. In this work, the sharp and intense bands at around 817 cm^{-1} for APMVO and 812 cm^{-1} for APZVO correspond to the stretching modes of the VO_4 groups, respectively. The substitution of the larger Zn^{2+} ions for smaller Mg^{2+} ions increases the unit cell volume, which further affects the inter atomic distance between the V–O tetrahedra. This result in higher ionic polarizability, and the vibrational modes shift toward the lower frequency side. The variation of relative permittivity with the Raman shift for some reported garnet compounds are plotted in Figure 8. It can be concluded that, generally for garnet systems, the vibrational Raman band shows a red shift with the increase in unit cell volume, which is attributed to the increase in bond length. A similar correlation between relative permittivity and Raman shift has also been observed in other systems, as reported by Wu et al.[51] in $Li_2Mg_3BO_6$ (B=Ti, Sn, Zr) and Zhang et al. in $Ba[Mg_{(1-x)/3}Zr_xTa_{2(1-x)/3}]O_3$.[54]

Figure 9 shows the variation of $Q_u \times f$ as the function of FWHM of symmetric stretching mode (A_{1g}) of compounds having the garnet structure. In general, garnet compounds with the lowest FWHM give the highest quality factor. Generally, FWHM is inversely related to the life time of the phonons, which indicates that a narrower band corresponds to a longer life time of the phonons and fewer interactions. As a result, the dielectric loss decreases and the quality factor increases. For example, the FWHMs of the $(V-O)$ stretching vibration for APMVO and APZVO are given in Table 3. APZVO shows the lowest FWHM for the symmetric stretching modes and the highest $Q_u \times f$ value compared to APMVO. It shows an inverse relation between the FWHM and the Q factor. A similar inverse relation between $Q_u \times f$ and FWHM of lattice vibration modes was reported by Wu et al. in $Li_2Mg_3BO_6$ (B=Ti, Sn, Zr) ceramics.[51] So, here the Raman shift and FWHM of the maximum-intensity bands are correlated with the microwave dielectric properties such as relative permittivity and quality factor for some reported garnet system. From this, it can be found that for compounds with high relative permittivity, the shift of vibrational band should be toward the lower frequency region in the Raman spectra, and also for better quality factor, the FWHM of A_{1g} mode should be minimum.

Another parameter that influences the quality factor of materials is its packing fraction. Kim et al.[55] have summarized the correlation between the Q factor and the packing fraction of structures.

Here, each ion in the crystal structure can be regarded as a rigid sphere. Packing fraction is defined as the ratio of the volume of ions in different sites to the total unit cell volume. The above authors reported that the increase in packing fraction could reduce the lattice vibrations, which results in high $Q_u \times f$. The packing fractions for $Pb_2AgB_2V_3O_{12}$ (B=Mg, Zn) can be calculated as follows:

$$\text{Packing fraction (\%)} = \frac{\text{volume of the packing ions}}{\text{volume of primitive unitcell}}$$

$$= \frac{\text{volumeofthe packing ions}}{\text{volume of unitcell}} \times \text{Z}$$

$$= \frac{\frac{4}{3}\pi[(r_{Ag^+})^3 + 2(r_{Pb^{2+}})^3 + 2(r_{B^{2+}})^3 + 3(r_{V^{5+}})^3 + 12\,(r_{O^{2-}})^3]}{a^3} \times Z \qquad (9)$$

The packing fraction increases as the unit cell volume decreases. Here, the observed a negative correlation between the packing fraction and $Q_u \times f$ implies that packing fraction is not the only factor that influences the quality factor of the material.

Bond valence is another important parameter that is bound up with microwave dielectric properties such as relative permittivity, $Q_u \times f$ and temperature coefficient of the resonant frequency. These parameters can be obtained through the following equations:

$$V = \sum v_{ij}$$

$$v_{ij} = \exp\left[\frac{R_{ij} - d_{ij}}{b}\right] \qquad (10)$$

Here, R_{ij} is the bond valence parameter for the cation–oxygen bond found in Brese's report[56], d_{ij} is the bond length between the B-site cations and oxygen ions found using the Rietveld refinement, and b is a universal constant equal to 0.37 Å. Table 4 shows the variation of relative permittivity, Q factor, and τ_f with the bond valence. When Mg^{2+} ions are replaced by Zn^{2+} ions, the bond valence as well as the bond strength increases slightly. Generally, in oxygen octahedra, when the bond valence between the cation and anion increases, it will create a more rigid octahedra, resulting in high bond strength. Also, it causes the decrease of rattling effect in the system, which in-turn decreases the permittivity of the materials.[57] Here, even though APZVO shows decreased rattling with increased bond strength, its

relative permittivity is slightly higher than that of APMVO. This may be due to the higher polarizability of Zn^{2+} (2.04 Å^3) compared to Mg^{2+} (1.32 Å^3) ions.

The bond valence of B-site cations can also influence the $Q_u \times f$ values of the compounds. As the bond valence increases, the damping constant of the microwave signal decreases because of the decrease in anharmonic interaction. These results in the lowering of the dielectric loss and better $Q_u \times f$.[58] In this work, we observe that the average B-site bond valence is higher for APZVO (1.933) than APMVO (1.938). These results in a slightly higher $Q_u \times f$ value for APZVO (28,400 GHz) compared to APMVO (26,900 GHz). Similar results on the variation of $Q_u \times f$ with A-site bond valence in $CaTiO_3$ were reported by Jimao et al.[57]

Another critical parameter determining the thermal stability of a dielectric material is the temperature coefficient of the resonant frequency (τ_f).The formula for τ_f with the temperature coefficient of dielectric constant (τ_ε) and linear thermal expansion coefficient (α_L) is as follows:

$$\tau_f = -[\frac{\tau_\varepsilon}{2} + \alpha_L] \qquad (11)$$

Here α_L can be taken as a constant (~ + 10 ppm/^{o}C) for all ceramic materials. Then, τ_f varies in proportion with the variation in τ_ε, which is a function of the structural characteristics such as the bond valence. The value of τ_f for APMVO is 19.3 and that of APZVO is –18.4. Table S5 shows the dependence of τ_f with sintering temperature. The higher value of $|\tau_f|$ for APMVO compared to APZVO is attributed to its lower bond valence. As the bond valence increases, the energy required to recover the structure increases, which results in low $|\tau_f|$ values. Similar results have been reported in $AgCa_2B_2V_3O_{12}$(B=Mg,Zn),[35]$(1–x)CaTiO_3–x(Li_{0.5}La_{0.5})TiO_3$,[57]and $Ca_5Zn_{4-x}Mg_xV_6O_{24}$ systems.[59]

4. CONCLUSIONS

The XRD patterns and vibrational spectra of $AgPb_2B_2V_3O_{12}$ (B=Mg, Zn) ceramics confirm the garnet structure of the compounds belonging to cubic symmetry with the space group $Ia\,\bar{3}$d. Using Rietveld analysis, the lattice parameters and bond lengths were obtained. As a general conclusion, the microwave dielectric properties of previously reported as well as $Pb_2AgB_2V_3O_{12}$ (B=Mg, Zn) ceramics correlate with the corresponding Raman shift and FWHM of the Raman bands. It was

observed that the vibrational modes of Raman spectra show a red shift with the increase in relative permittivity. The lowest FWHM of symmetric stretching mode (A_{1g}) results in the highest quality factor. Also for APZVO, as the bond valence increases, $Q_u \times f$ increases and $|\tau_f|$ decreases because of the stronger bond between the cation and oxygen ions, which decreases the anharmonic interactions and increases the energy used to recover the structural distortion caused by oxygen polyhedra. APZVO shows a higher relative permittivity than APMVO, which is due to its larger ionic polarizability. As a result, APMVO has a porosity-corrected relative permittivity of 23.3 ± 0.2 and, a high quality factor ($Q_u \times f$) of around $26{,}900 \pm 500$, and a positive temperature coefficient of resonant frequency of 19.3 ± 1 ppm/^{o}C at its optimized sintering temperature. Meanwhile, APZVO ceramic has a higher relative permittivity of 26.4 ± 0.2, unloaded quality factor of $28{,}400 \pm 500$ GHz, and temperature coefficient of resonant frequency of -18.4 ± 1 ppm/^{o}C, which makes it a promising candidate for future microwave electronic applications.

ACKNOWLEDGMENTS

Financial support from Alexander von Humboldt foundation, Germany, through an equipment grant is acknowledged. This work was financially supported by the SRS program of KSCSTE.

REFERENCES

1. Zhang J, Yue ZX, Zhou YY, et al. Microwave dielectric properties and thermally stimulated depolarization currents of (1-x) $MgTiO_3$–x$Ca_{0.8}Sr_{0.2}TiO_3$ ceramics. J Am Ceram Soc. 2015;98: 1548-1554.

2.Lei SH, Fan HQ, Ren XH, et al. Novel sintering and band gap engineering of $ZnTiO_3$ ceramics with excellent microwave dielectric properties. J Mater Chem C. 2017;5:4040-4047.

3.Luo H, Fang W, Fang L, Li W, Li C, Tang Y. Microwave dielectric properties of novel glass-free low temperature firing $ACa_2Mg_2V_3O_{12}$ (A=Li, K) ceramics. Ceram Inter.2016;42: 10506–10510.

4. Krzmanc MM, Logar M, Budic B, Suvorov D. Dielectric and micro structural study of the $SrWO_4$, $BaWO_4$, and $CaWO_4$ Scheelite ceramics. J Am Ceram Soc. 2011;94:2464–2472.

5. Zhou D, Wang H, Yao X, Pang LX. Sintering behavior, phase evolution, and microwave dielectric properties of Bi ($Sb_{1-x}Ta_x$) O_4 ceramics. J Am Ceram Soc. 2008;91:2228–2231.

6.Subodh G, Ratheesh R, Jacob MV, Sebastian MT. Microwave dielectric properties and vibrational spectroscopic analysis of $MgTe_2O_5$ ceramics. J Mater Res. 2008;23(6):1551-1556.

7. Subodh G, Sebastian MT. Glass-Free $Zn_2Te_3O_8$ Microwave Ceramic for LTCC Applications. J Am Ceram Soc. 2007;90(7):2266–2268.

8. Pang L, Zhou D, Qi ZM, Yue ZX. Influence of W substitution on crystal structure, phase evolution and microwave dielectric properties of ($Na_{0.5}Bi_{0.5}$) MoO_4 ceramics with low sintering temperature. Sci Rep. 2017;7:3201-3204.

9. George S, Sebastian MT. Synthesis and Microwave Dielectric Properties of Novel Temperature Stable High Q, $Li_2ATi_3O_8$ (A=Mg, Zn) Ceramics. J Am Ceram Soc.2010;93(8): 2164–2166.

10. Kwon DK, Lanagan MT, Shrout TR. Microwave Dielectric Properties of BaO-TeO_2 Binary Compounds. Mater Lett. 2007;61:1827–1831.

11. Udovic M, Valant M, Suvorov D. Phase Formation and Dielectric Characterization of the Bi_2O_3-TeO_2 System Prepared in an Oxygen Atmosphere. J Am Ceram Soc. 2004;87(4):591–597.

12. Valant M, Suvorov D. Processing and Dielectric Properties of Sillenite Compounds $Bi_{12}MO_{20}$ (M=Si, Ge, Ti, Pb, Mn, $B_{1/2}P_{1/2}$). J Am Ceram Soc. 2001;84(12):2900–2904.

13. Zhou D, Wang H, Pang LX, Randall CA, Yao X.Bi_2O_3-MoO_3 Binary System: An Alternative Ultralow Sintering Temperature Microwave Dielectric. J Am Ceram Soc. 2009;92(10): 2242–2246.

14. Zhou D, Randall CA, Wang H, Pang L-X, Yao X. Microwave Dielectric Ceramics in Li_2O-Bi_2O_3-MoO_3 System with Ultra low Sintering Temperature. J Am Ceram Soc. 2010;93(4):1096–1100.

15. Sebastian MT, Solomon S, Ratheesh R. Preparation, Characterization, and Microwave Properties of $RETiNbO_6$ (RE = Ce, Pr, Nd, Sm, Eu, Gd, Tb, Dy, Y, and Yb) Dielectric Ceramics. J Am Ceram Soc. 2001;87(7):1487-1489.

16. Sreemoolanadhan H, Sebastian MT, Mohanan P. Dielectric Ceramics in the $BaO.Ln_2O_3.5TiO_2$Composition. Ferroelectrics 1996;189:43-46.

17.MengSQ, Yue ZX, Zhuang H, Zhao F, Li LT. Microwave dielectric properties of $Ba_3(VO_4)_2$ Mg_2SiO_4 composite ceramics. J Am. Ceram Soc. 2010;93:359-361

18. Induja IJ, Sebastian MT. Microwave dielectric properties of mineral sillimanite obtained by conventional and cold sintering process. J Eur Ceram. Soc. 2017;37:2143-2147.

19.Song KX, Liu P, Lin HX, et al. Symmetry of hexagonal ring and microwave dielectric properties of $(Mg_{1-x}Ln_x)_2Al_4Si_5O_{18+x}$(Ln=La, Sm) cordierite-type ceramics. J Eur Ceram Soc. 2015; 36:1167-1175.

20. Manu KM, Joseph T, Sebastian MT. Temperature compensated $Sr_2Al_2SiO_7$ ceramic for microwave applications. Mater Chem Phys. 2012;133:21-23.

21. Kudo A, Omori K, Kato H. A Novel Aqueous Process for Preparation of Crystal Form-Controlled and Highly Crystalline $BiVO_4$ Powder from Layered Vanadates at Room Temperature and Its Photocatalytic and Photophysical Properties. J Am ChemSoc. 1999;121:11459−11467.

22. Pope M T, Muller A. Polyoxolometalate Chemistry - An Old Field with New Dimensions in Several Disciplines. Angew Chem IntEd Engl. 1991;30:34−48.

23. Rupert PB. Transition State Stabilization by a Catalytic RNA. Science 2002;298: 1421−1424.

24. Nakajima T, Isobe M, Tsuchiya T, Ueda Y, Manabe T. Correlation between Luminescence Quantum Efficiency and Structural Properties of Vanadate Phosphors with Chained, Dimerized, and Isolated VO_4 Tetrahedra. J Phys ChemC. 2010;114:5160−5167.

25. Nakajima T, Isobe M, Tsuchiya T. Rare Earth-Free High Color Rendering White Light-Emitting Diodes Using $CsVO_3$ with Highest Quantum Efficiency for Vanadate Phosphors. J Mater Chem C. 2015;3:10748−10754.

26.Wang Y, Zuo R, Zhang C, Zhang J, Zhang T. Low - temperature - fired $ReVO_4$(Re = La, Ce) microwave dielectric ceramics. J Am Ceram Soc. 2015;98(1):1-4.

27. Li B, Zheng J, Li W. Enhanced effect of vanadium ions non-stoichiometry on microwave dielectric properties of $Ca_5Co_4V_{6+x}O_{24}$ceramics.J Mater Chem and Phys. 2018;207:282-288.

28. Yao GG, Pei CJ, Liu P, Zhou JP, Zhang HW. Microwave dielectric properties of low temperature sintering $Ca_5Mn_4(VO_4)_6$, ceramics. J Mater Sci- Mater Electr.2016;27:7292-7296.

29. Zhou D, Li J, Pang LX, Wang DW, Reaney IM. Novel water insoluble (Na_xAg_{2-x})MoO_4($0 \leq x \leq 2$) microwave dielectric ceramics with spinel structure sintered at 410 degrees. J Mater Chem C. 2017;5:6086-6091.

30. Zhou H, Miao Y, Chen J, Chen X, He F, Ma D. Sintering characteristic, crystal structure and microwave dielectric properties of a novel thermally stable ultra-low-firing $Na_2BiMg_2V_3O_{12}$ ceramic. J Mater Sci - Mater Electr.2014;25:2470–2474.

31. Hasegawa T, Abe Y, Koizumi A, Ueda T, Toda K, Sato M. Bluish-White Luminescence in Rare-Earth-Free Vanadate Garnet Phosphors: Structural Characterization of $LiCa_3MV_3O_{12}$(M = Zn and Mg). Inorg Chem. 2018;57:857−866.

32. Liang F, Fei X, Congxue S, Hui Z. A Novel Low Firing Microwave Dielectric Ceramic $NaCa_2Mg_2V_3O_{12}$. Ceram Int. 2013;39(8):9779–9783.

33. Fang L, Su CX, Zhou HF, Wei ZH, Zhang H. Novel Low-Firing Microwave Dielectric Ceramic $LiCa_3MgV_3O_{12}$ with Low Dielectric Loss. J Am Ceram Soc.2013**; 96**:688-690.

34. Yao GG, Liu P, Zhang HW. Novel Series of Low-Firing Microwave Dielectric Ceramics: $Ca_5A_4(VO_4)_6$ (A^{+2} = Mg, Zn). J Am Ceram Soc. 2013;96(6):1691–1693.

35. Chen J, Tang Y, Xiang H, Fang L, Porwal H, Li C. Microwave dielectric properties and infrared reflectivity spectra analysis of two novel low-firing $AgCa_2B_2V_3O_{12}$ (B=Mg, Zn) ceramics with garnet structure. J Eur Ceram Soc.2018;38(14):4670-4676.

36. Rakhi M, Subodh G. Crystal structure and microwave dielectric properties of $NaPb_2B_2V_3O_{12}$(B=Mg, Zn) ceramics. J Eur Ceram Soc. 2018;38:4962–4966.

37. Iishi K, Ikuta Y. Isomorphous substitutions in vanadate garnets. NJb Miner Abh. 2006;182(2):157-163.

38. Osipov, A.A, Osipova L.M. Raman scattering study of barium borate glasses and melts.J Phys and Chem Solids. 2013;74 971–978.

39. Hawthorne F. C. Some Systematics of the Garnet Structure. J Solid State Chem. 1981;37: 157−164.

40. Huang Y, Yu YM, Tsuboi T, Seo HJ. Novel Yellow- Emitting Phosphors of $Ca_5M_4(VO_4)_6$ (M = Mg, Zn) with Isolated VO_4Tetrahedra. Opt Express 2012;20:4360−4368

41. Koningstein JA, Mortensen OS, Laser-Excited Phonon Raman Spectrum of Garnets. J Mol Spectrosc.1968;27:343-350.

42. Moore RK, White WB, Long TV. Vibrational spectra of the common silicates. I. Garnets. Am Mineral. 1971;56:54-71.

43. White WB, Keramidas VG. Raman Spectra of Yttrium Iron Garnet and two vanadium Garnets. J Am Ceram Soc. 1971;54:472-473.

44. Liu H, Yuan L, Wang S, Fang H, Zhang Y, Hou C, Feng S. Structure, optical spectroscopy properties and thermochromism of $Sm_3Fe_5O_{12}$ garnets. J Mater Chem C.2016; 4:10529-10537.

45. Hofmeister AM, Campbell KR. Infrared spectroscopy of yttrium aluminum, yttrium gallium, and yttrium iron garnets. J Appl Phys. 1992;72:638-646.

46. Yoon SH, Kim DW, Cho SY, Hong KS. Investigation of the relations between structure and microwave dielectric properties of divalent metal tungstate compounds. J Eur Ceram Soc. 2006;26:2051-2054.

47. Xiao M, Lou J, Wei Y, Zhang P. Crystal structure and microwave dielectric properties of $MgZr_{1-x}Sn_xNb_2O_8$ ceramics. Ceram Int. 2018;44:885–889.

48. Liao Q, Li L, Ren X, Ding X. New Low-Loss Microwave Dielectric Material $ZnTiNbTaO_8$. J Am Ceram Soc. 2011;94(10):3237–3240.

49.Butee S, Kulkarni AR, Prakash, R.P.R.C. Aiyar, Wattmwar I, Bais D, Sudheeran K, James RKC. Significant Enhancement in Quality Factor of Zn_2TiO_4 with Cu-Substitution. Mater Sci Eng B. 2011;176(7):567–572.

50. Shannon RD. Dielectric polarizability of ions in oxides and fluorides. J Appl Phys. 1993;73: 348–366.

51. Wu H, Kim ES. Correlations between crystal structure and dielectric properties of high-*Q* materials in rock-salt structure Li_2O–MgO–BO_2 (B = Ti, Sn, Zr) systems at microwave frequency.RSC Adv. 2016;6:47443-47453.

52. Jo HJ, Kim ES. Effects of structural characteristics on microwave dielectric properties of $MgTi_{1-x}(Mg_{1/3}B_{2/3})xO_3$(B = Nb, Ta). J Eur Ceram Soc. 2016;36:1399–1405.

53. Zhou D, Li J, Pang L-X et al. Crystal Structure, Infrared Spectra, and Microwave Dielectric Properties of Temperature-Stable Zircon-Type (Y,Bi)VO_4 Solid Solution Ceramics. ACS Omega. 2016;1:963-970.

54. Zhang H, Diao C, Liu S, Jiang S, Shi F, Jing X. X-ray diffraction and Raman scattering investigations on $Ba[Mg(1-x)/_3Zr_xTa_2(1-x)/_3]O_3$ solid solutions. J Alloys Compd. 2014;587:717-723.

55. Kim ES, Chun BS, Freer R, Cernik RJ. Effects of packing fraction and bond valence on microwave dielectric properties of $A^{2+}B^{6+}O_4$ (A^{2+}: Ca, Pb, Ba; B^{6+}: Mo, W) ceramics. J Eur Ceram Soc.2010;30:1731–1736.

56. B.N.E. Brese, O'Keeffe M. Bond-valence parameters for solids. Acta Cryst. B47 1991;192–197.

57.Li J, Han Y, Qiu T, Chuangui Jin C. Effect of bond valence on microwave dielectric properties of$(1 -x)CaTiO_3–x(Li_{0.5}La_{0.5})TiO_3$ ceramics. Mater Res Bull. 2012;47:2375–2379.

58. Singh SK, Murthy VRK. Crystal structure, Raman spectroscopy and microwave dielectric properties of layered-perovskite $BaA_2Ti_3O_{10}$ (A = La, Nd and Sm) Compounds. Mater Chem Phys. 2015;160:187-193

59. Li B, Tian J, Qiu L. Crystal structures and microwave dielectric properties of low-firing $Ca_5Zn_{4-x}Mg_xV_6O_{24}$ ceramics. Ceram Inter. 2018;44:18250–18255.

Table Captions

Table 1. Crystallographic parameters obtained from Rietveld refinement of the XRD pattern of APMVO ceramic.

Atom	**Site**	***x***	***y***	***z***	**Occupancy**	B_{eq}**(Å^2)**
Pb1	24*c*	0.37500	0.50000	0.25000	0.6667	0.8998
Ag1	24*c*	0.37500	0.5000	0.25000	0.3333	0.9000
Mg1	16*a*	0.50000	0.50000	0.00000	1	0.6125
V1	24*d*	0.62500	0.50000	0.25000	1	0.4579
O1	96*h*	0.04200	0.04710	0.65290	1	0.758

Table 2. Crystallographic parameters obtained from Rietveld refinement of the XRD pattern of APZVO.

Atom	**Site**	***x***	***y***	***z***	**Occupancy**	B_{eq} **(Å^2)**
Pb1	24*c*	0.37500	0.50000	0.25000	0.6667	0.9099
Ag1	24*c*	0.37500	0.50000	0.25000	0.3333	0.7501
Zn1	16*a*	0.50000	0.50000	0.00000	1	0.6510
V1	24*d*	0.62500	0.50000	0.25000	1	0.4957
O1	96*h*	0.04053	0.04800	0.6531	1	0.758

Table 3 FWHM of symmetric stretching modes (A_{1g}), theoretical and observed polarizability, packing fraction, and microwave dielectric properties.

Sample name	Raman shift (cm^{-1})	FWHM (cm^{-1})	α_{theor}	Relative permittivity (ε_r)	Porosity corrected (ε_r)	α_{obs}	Packing fraction	$Q_u \times f$ (GHz)	τ_f (ppm/ ^oC)
APMVO	817	28.5	50.9	22.3 ± 0.2	23.3 ± 0.2	54.4	64.7	$26{,}900 \pm 500$	19.3 ± 1
APZVO	812	24.2	52.4	24.4 ± 0.2	26.4 ± 0.2	55.3	64.5	$28{,}400 \pm 500$	-18.4 ± 1

Table 4. Bond lengths, bond valence, and microwave dielectric properties of APMVO and APZVO ceramics.

Compound	Octahedral bond type	Bond length (d_{ij}) in Å	Bond valence parameter (R_{ij})	Bond valence (V)	Porosity-corrected relative permittivity (ε_r)	$Q_u \times f$ (GHz)	τ_f (ppm/ ^oC)
$AgPb_2Mg_2V_3O_{12}$	Mg–O	2.111(9)	1.693	1.933	23.3 ± 0.2	26,900 $\pm$ 500	19.3 $\pm$ 1
$AgPb_2Zn_2V_3O_{12}$	Zn–O	2.122(1)	1.704	1.938	26.4 ± 0.2	28,400 $\pm$ 500	-18.4 $\pm$ 1

Figure Captions

Figure 1.Rietveld refinement of X-ray diffraction pattern of APMVO ceramics calcined at 625 ^{o}C.

Figure 2.Rietveld refinement of X-ray diffraction pattern of APZVO ceramics calcined at 550 ^{o}C.

Figure 3.Dependence of bulk density and relative density on sintering temperature for APMVO and APZVO ceramics

Figure 4.Microstructures of (a) APMVO and (b) APZVO sintered at 750 and 590 ^{o}C, respectively.

Figure 5.Deconvoluted Raman spectra of APMVO and APZVO ceramics calcined at 625 and 550 ^{0}C. Experimental data are in olive colored solid circles, while the fitting curve is the green line. Red line represents the phonon modes fitted using a Lorentzian function.

Figure 6.Dependence of the relative permittivity and $Q_u \times f$ on sintering temperature for APMVO ceramic sintered at 750 ^{o}C.

Figure 7.Dependence of the relative permittivity and $Q_u \times f$ on sintering temperature for APZVO ceramic sintered at 590 ^{o}C.

Figure 8.Variations of relative permittivity with Raman shift for few reported garnet systems.

Figure 9.Variation of $Q_u \times f$ as a function of FWHM of symmetric stretching mode (A_{1g}) of reported garnet compounds.

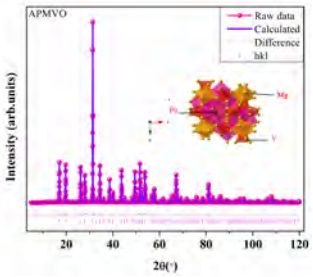

jace_16991_f1.tif

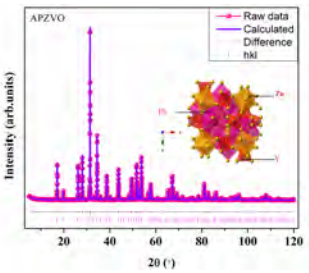

jace_16991_f2.tif

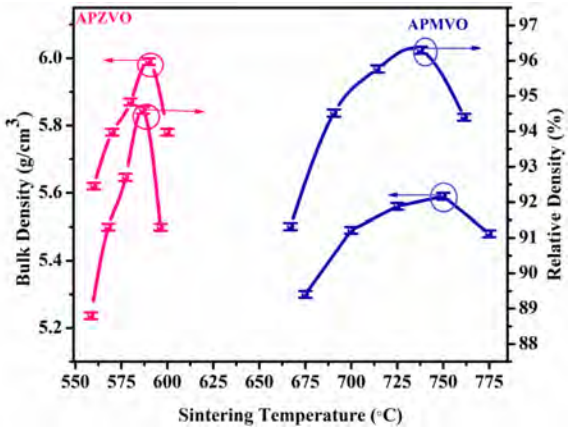

jace_16991_f3.tif

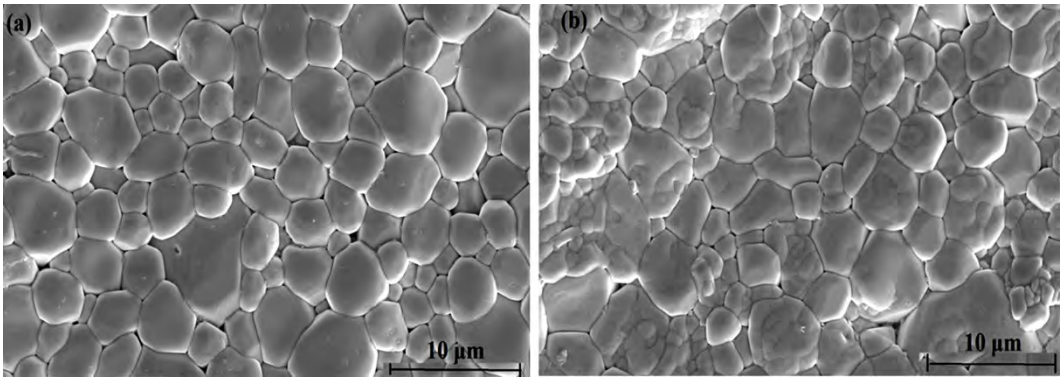

jace_16991_f4.tif

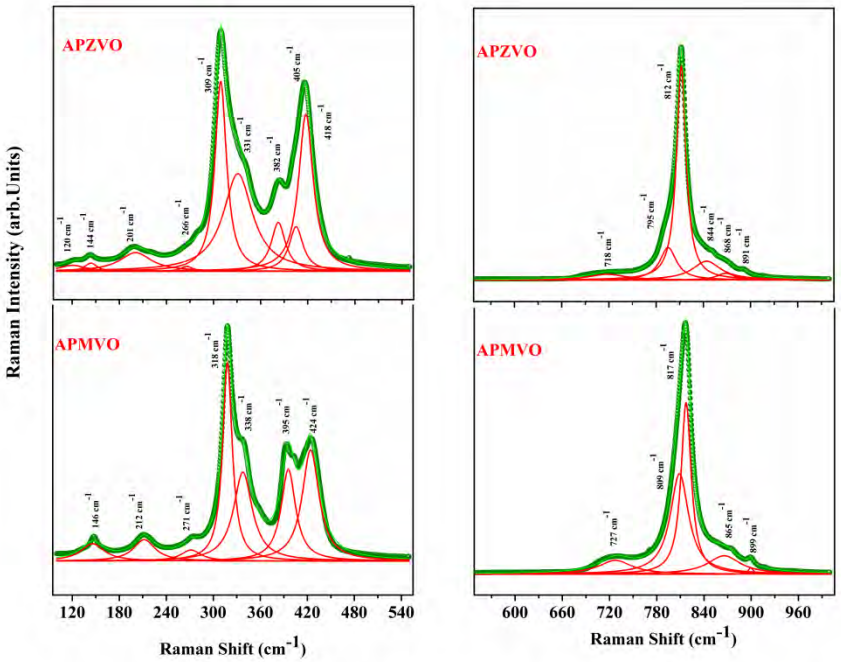

jace_16991_f5.tif

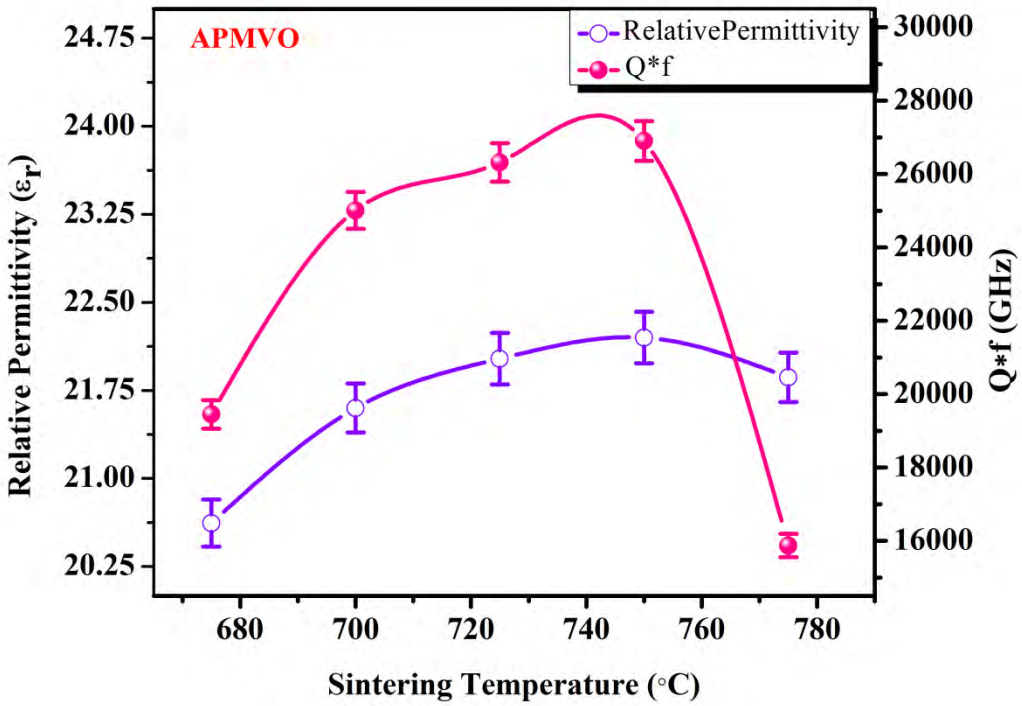

jace_16991_f6.tif

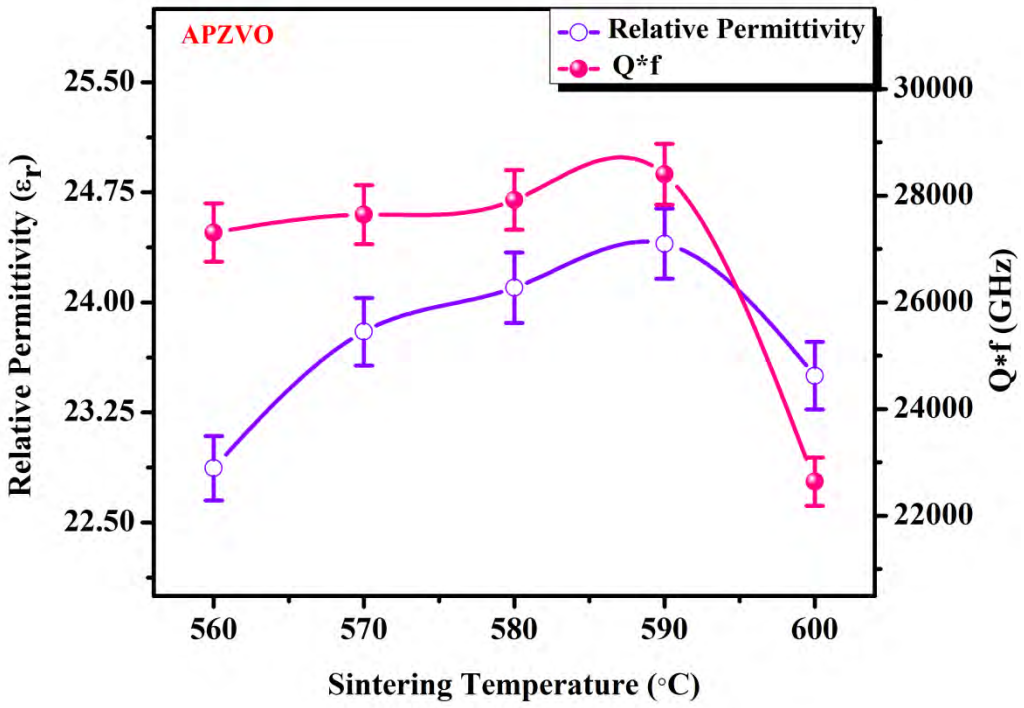

jace_16991_f7.tif

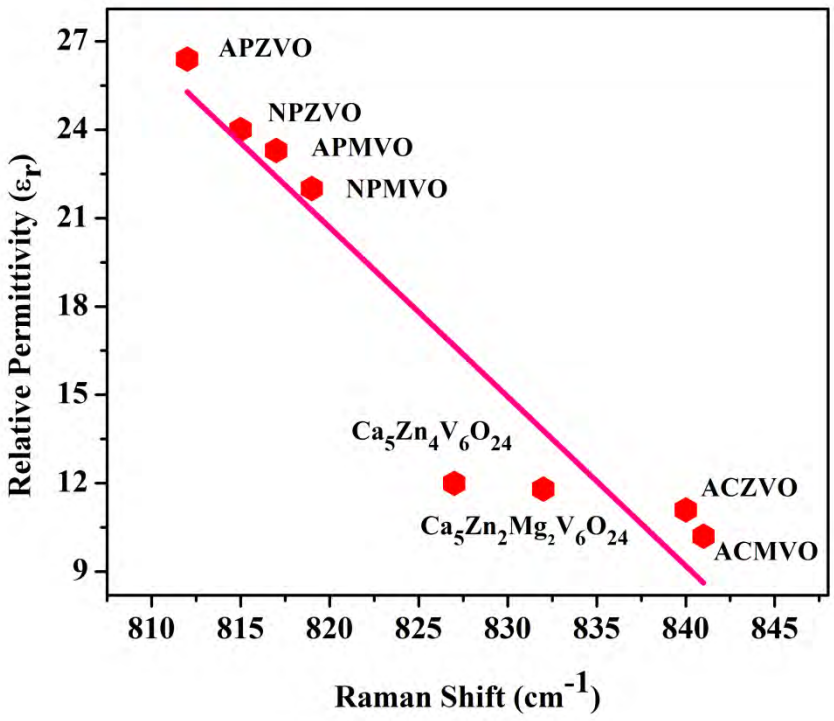

jace_16991_f8.tif

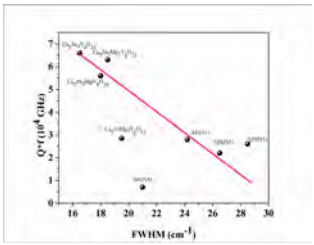

jace_16991_f9.tif